Immediate elimination of injured white matter tissue achieves a rapid axonal growth across the severed spinal cord in adult rats

AUTHOR(S):

Nishio, Takeshi; Fujiwara, Hiroshi; Kanno, Isaku

CITATION:

Nishio, Takeshi ...[et al]. Immediate elimination of injured white matter tissue achieves a rapid axonal growth across the severed spinal cord in adult rats. Neuroscience Research 2018, 131: 19-29

ISSUE DATE:

2018-06

URL:

http://hdl.handle.net/2433/233092

Neuroscience Research 131 (2018) 19–29

Contents lists available at ScienceDirect

Neuroscience Research

journal homepage: www.elsevier.com/locate/neures

Immediate elimination of injured white matter tissue achieves a rapid axonal growth across the severed spinal cord in adult rats

Takeshi Nishio [a,*], Hiroshi Fujiwara [b], Isaku Kanno [c]

[a] Department of Integrative Brain Science, Kyoto University Graduate School of Medicine, Yoshida-Konoe, Sakyo, Kyoto 606-8501, Japan
[b] Department of Obstetrics and Gynecology, Kanazawa University Graduate School of Medical Sciences, Takara-Machi 13-1, Kanazawa 920-8641, Japan
[c] Department of Mechanical Engineering, Kobe University, Rokkodai-cho 1-1, Nada-ku, Kobe 657-8501, Japan

ARTICLE INFO

Article history:
Received 18 July 2017
Received in revised form 8 October 2017
Accepted 26 October 2017
Available online 10 November 2017

Keywords:
Regenerative pioneering axon
Regenerative follower axon
Axon-glial complex
Debridement
Fascicle formation
Axon segments (fragments)

ABSTRACT

In general, axonal regeneration is very limited after transection of adult rat spinal cord. We previously demonstrated that regenerative axons reached the lesion site within 6 h of sharp transection with a thin scalpel. However, they failed to grow across the lesion site, where injured axon fragments (axon-glial complex, AGC) were accumulated. Considering a possible role of these axon fragments as physicochemical barriers, we examined the effects of prompt elimination of the barriers on axonal growth beyond the lesion site. In this study, we made additional oblique section immediately after the primary transection and surgically eliminated the AGC (debridement). Under this treatment, regenerative axons successfully traversed the lesion site within 4 h of surgery. To exclude axonal sparing, we further inserted a pored sheet into the debrided lesion and observed the presence of fascicles of unmyelinated axons traversing the sheet through the pores by electron microscopy, indicating *bona fide* regeneration. These results suggest that the sequential trial of reduction and early elimination of the physicochemical barriers is one of the effective approaches to induce spontaneous and rapid regeneration beyond the lesion site.

1. Introduction

After a transection of the white matter in adult mammalian central nervous system (CNS), severed axons show a rapid retraction within 0.5–1 h of axotomy and then attempt regeneration in 6 h (Ramon y Cajal, 1928; Kerschensteiner et al., 2005; Nishio et al., 2008). However, axon regeneration is very limited in adult CNS because regenerative axons hardly grow across the lesion site (Silver and Miller, 2004; Busch and Silver, 2007; Schwab and Strittmatter, 2014).

Regarding the cause of limited regeneration, the presence of several types of axon growth inhibitory molecules have been shown in adult mammalian CNS, such as myelin-associated inhibitors (Schwab and Strittmatter, 2014) or glial scar-related extracellular matrix molecules (Silver and Miller, 2004; Busch and Silver, 2007; Sharma et al., 2012). However, the real cause remains elusive. The evidence that adult dorsal root ganglion neurons that were implanted into the spinal cord of adult rats can robustly regenerate their axons along the myelin-rich white matter tracts (Davies et al., 1999) may cast a doubt on the idea of myelin-inhibition *in vivo*. Furthermore, a glial scar takes several days to form after CNS injuries (Silver and Miller, 2004), while severed axons start regeneration within 6 h (Ramon y Cajal, 1928; Kerschensteiner et al., 2005; Nishio et al., 2008). If regenerative axons reach the lesion site before a scar formation, a structure other than a glial scar would be associated with the growth inhibition of such rapidly regenerating axons (regenerative pioneering axons).

We have previously reported a successful regeneration of the corticospinal tract after a sharp transection of the cord in young rats (Iseda et al., 2003; Iseda et al., 2004). In those animals, regenerative axons rapidly traversed the lesion site within 12–18 h of a sharp section and later a glial scar did not take place at the lesion site, while regeneration failed after a more traumatic injury and a glial scar was later formed. Therefore, the spatiotemporal correlation of these events suggests that a glial scar would follow, rather than cause, the failure of regeneration and that a local environment at the lesion site during the first several hours of injury would determine the fate of regenerative pioneering axons in young rats.

In cordotomized adult rats, we previously found an early access, within 6 h, of the regenerative pioneering axons to the lesion site,

Abbreviations: AGC, axon-glial complex; BSA, bovine serum albumin; CNS, central nervous system; DxRh, dextrans conjugated with tetramethylrhodamine; Dx488, dextrans conjugated with Alexa Fluor 488; IR, immunoreactivity; GM, gray matter; NFH, high-molecular-weight neurofilament subunit; GFAP, glial fibrillary acidic protein; PBS, phosphate buffered saline; WM, white matter; YG, yellow green.

* Corresponding author.
E-mail address: nishio.takeshi.5m@kyoto-u.ac.jp (T. Nishio).

https://doi.org/10.1016/j.neures.2017.10.011

where abnormal zipper-like axon segments were formed within a few hours of severance with a fine scalpel (Nishio et al., 2008). By extension of the view in young rats, we hypothesized that the axon segments would be a barrier for the regenerative pioneering axons in adult rats. In the present study, we further characterized the regenerative pioneering axons and the abnormal axon segments using axonal tracings, immunofluorescence, and electron microscopy. To verify this hypothesis, we developed a novel surgical treatment to eliminate the axon segments and examined whether a successful regeneration would occur under the barrier-eliminating surgery or not. Fortunately, we achieved a successful regeneration under the barrier-eliminating surgery.

However, in studies showing *in vivo* regeneration of CNS axons, the "spared axon problem", in which axons that survive a lesion are mistakenly identified as having regenerated, comes often to an issue (Steward et al., 2003). Therefore, we adopted several methods according to the criteria for identifying regenerated axons in injured spinal cord (Steward et al., 2003). To be specific, according to the criterion (II: the axon extends from the host CNS into a non-host graft or transplant), we inserted an artificial sheet or injected immobile microspheres into the lesion site to allow regeneration across the nonhost sheet or microspheres. According to the criteria (IV: the axon takes an unusual course through the tissue environment of the CNS, VI: the axon is tipped with a growth cone, VII: the axon has a morphology that is not characteristic of normal axons of its type), we characterized morphological features of regenerative pioneering axons, which could distinguish regenerative axons from normal ones.

2. Materials and methods

2.1. Animals

All procedures were in compliance with NIH guidelines and were approved by the Animal Care and Use Committee of Graduate School of Medicine, Kyoto University (No. 12036), and all efforts were made to minimize the number of animals used and their suffering. Adult female rats of Sprague-Dawley strain (60–70 days of age, N = 31) were used. Animals receiving a single transection of the cord were subjected to a quantitative analysis (N = 7, survival time was 2 and 4 h), to an immunofluorescence (N = 6, survival time was 2 and 6 h), and to an electron microscopy (N = 3, survival time was 2 h). Animals receiving cord sections with a local tissue removal (N = 6, survival time was 1 and 4 h), receiving cord sections with a local tissue removal plus a microsphere injection (N = 3, survival time was 4 h), or receiving cord sections with a local tissue removal plus a sheet insertion (N = 6, survival time was 24 h) were subjected to histologic processing described below.

2.2. Surgical procedures

After an intra-peritoneal anesthesia with sodium pentobarbital (25 mg/kg), laminectomies, pediculectomies and a dural incision were done to expose a dorsolateral surface of the lower thoracic cord (T8-12) under a surgical microscope (OPMI CS-NC, Contraves, Carl Zeiss Germany). The exposure of many segments of cord was required for a local axonal labeling as described below. The lateral funiculus was cut at T10 level on the left side with a disposable ophthalmic scalpel (microfeather P-715, Feather Safety Razor Co. Ltd, Osaka, JAPAN). The wound was gently closed in animals of a single transection.

We developed a novel surgical procedure to remove the abnormal axon fragments or axon-glial complex at the lesion site. Immediately after the primary section (lateral funiculotomy), an oblique section of the left lateral funiculus was added at the site 300–500 μm caudal to the primary lesion (cutting angle was about 30° to the primary section). Then, the intervening tissue between the 2 sections was removed. In addition, the surface of both stumps was carefully debrided with a pair of tweezers under a visual guidance (surgical debridement). The widely open cut stumps were closed by drawing a dura mater or nerve roots and held stable for 10 min to induce immediate tissue adhesion (see Supplementary Video online). To effectively perform the above surgery, we precoated the pial surface with a surgical adhesive [mixture of bovine serum albumin (BSA) and glutaraldehyde].

2.3. Fluorescent microspheres

Fluorescent microspheres (Fluoresbrite YG microsphere 3.0 μm #17155, Polysciences, Inc. 400 Valley Road, Warrington, PA) were coated with BSA by soaking them overnight in a 20% BSA solution. The BSA-coated microspheres (0.3 μl of 2.5% aqueous suspension) were manually injected into the tissue-removed space through a glass micropipette at a rate of 0.05 μl per a minute.

2.4. Epoxy-based sheets with pores

SU-8 photoresist coated on Al-coated glasses was exposed to UV light through a photo-mask of dot pattern of 125 μm in diameter. After curing them at 350 °C, 19.6 μm-thick SU-8 layer with 125 μm pores and 150 μm pitch was prepared on the glass substrates. Finally, the epoxy-based SU-8 sheets were peeled off from the glass substrates. The 19.6 μm-thick epoxy-based sheet ($575 \times 475\ \mu m^2$) was inserted into the tissue-removed space with a pair of tweezers under a visual guidance. The epoxy-based sheet was left at the lesion site until the histological processing, during which a frozen cord with the sheet was cut at 50-μm width by a freezing microtome for immunohistology, or a fixed cord with the sheet was cut at 70 nm width by an ultra-microtome for electron microscopy.

2.5. Local axonal tracing

Axons in the left lateral funiculus were labeled with an aldehyde-fixable fluorescent tracer (0.1 μl of 20% solution, dextrans conjugated with tetramethylrhodamine, DxRh, D-3308, or dextrans conjugated with Alexa Fluor 488, Dx488, D22910, Molecular Probes, Inc. Thermo Fisher Scientific, USA). Immediately after the surgery, rats were manually injected with the tracer solution into the lateral funiculus through a glass micropipette at a rate of 0.05 μl per a minute. In a preliminary study, a maximal distance of axonal labeling from an injection point was 4.5 mm at an hour, 5.6 mm at 2 h, 7.8 mm at 4 h and 9.6 mm at 6 h post-injection. Thus, the tracer was injected 4 mm rostral (or caudal) to the lesion site in animals who would survive 1 or 2 h of surgery, and 5 mm rostral (or caudal) to the lesion site in animals who would survive 4 h or more of surgery.

2.6. Histological processing and immunofluorescence

The immunohistological procedures were described elsewhere (Kawasaki et al., 2003; Nishio et al., 2005; Nishio et al., 2008). Briefly, rats were anesthetized with sodium pentobarbital (60 mg/kg, i.p.) and were fixed by transcardiac purfusion with 4% paraformaldehyde in 0.1 M phosphate buffered saline (PBS, pH 7.4). The spinal cords were removed and subjected to postfixation with the same fixative overnight at 4° C. They were cryoprotected with 20% sucrose in 0.1 M PBS at 4° C. Frozen thoracic cord was cut at 50-μm width in a horizontal plane or in a parasagittal plane by a freezing microtome. All serial 50-μm sections were preserved in 0.1 M PBS at 4° C in 96-well plate. For the antigen exposure,

they were treated with PBS containing 0.3% Triton X-100 (PBS-Triton) for 48 h at 4° C. They were incubated in a free-floating state for 48 h at 4° C in PBS-Triton containing primary antibodies. After rinse, they were incubated at 4° C overnight in PBS-Triton containing the following affinity-purified second antibodies absorbed for dual labeling; Alexa Fluor 488-conjugated goat anti-mouse IgG (2 μg/ml, A-11029, Molecular Probe, Thermo Fisher Scientific), Alexa Fluor 488-conjugated goat anti-rabbit IgG (2 μg/ml, A-11034, Molecular Probe, Thermo Fisher Scientific), Cy3-conjugated donkey anti-mouse IgG (2 μg/ml, AP192C, Chemicon, Merck-Millipore, USA). The staining specificity was assessed by omission of the primary antibody or incubation with normal rabbit serum as the primary antibody.

2.7. Primary antibodies

Used primary antibodies for immunofluorescence were as follows. Mouse monoclonal antibody against glial fibrillary acidic protein (1/400, G3893, clone G-A-5, Sigma-Aldrich Co. LLC), mouse monoclonal antibody against neurofilament (200 kDa) (1/500, clone RT97, MAB5262, Chemicon, Merck-Millipore), mouse monoclonal antibody against neuronal class III beta-tubulin (1/500, clone TUJ1, Covance Research Products Inc. Berkeley, CA 94710, U.S.A.), rabbit polyclonal antibody against neurofilament (200 kDa) (1/400, AB1982, Chemicon, Merck-Millipore).

2.8. Electron microscopy

Animals (N = 3) 2 h of a lateral funiculotomy or animals (N = 3) 24 h of duplicated cord sections, tissue removal, and sheet insertion were fixed through a transcardiac perfusion with 2.5% glutaraldehyde in 0.1 M phosphate buffer, pH 7.4. The fixed spinal cord tissue including the lesion was cut into a 2-mm segment, which received post-fixation with 1% osmium tetraoxide. Ultrastructure at the lesion site was analyzed under JEM1010 electron microscope (JOEL, Tokyo, Japan).

2.9. Image analysis

The labeled sections were observed under a fluorescent microscope (IX-70, Olympus, Tokyo, Japan) with 3 filter cubes, U-MNIBA, U-DM-Cy3 and U-DM-Cy5. The observed images were digitally processed with image analyzing software Openlab 2.2 (Improvision, Coventry, England). For spatial resolution, they were also analyzed under a fluorescence microscope (Axiophot2, Carl-Zeiss, Germany) equipped with a laser scanning confocal imaging system MRC-1024 (BIO-RAD, Hercules, CA, U.S.A.). Triple labeling with Alexa Fluor 448, rhodamine (or Cy3) and Cy5 was excited at 488 nm, 568 nm and 647 nm emitted from Krypton/Argon mixed gas laser. Each emission passed through a filter of 522DF32, 605DF32 or 680DF32 was analyzed with a laser scanning confocal imaging system MRC-1024.

2.10. Quantitative image analysis

Horizontal spinal cord sections (50 μm in width) including the lesion and axonal labeling in the left lateral funiculus were selected under the fluorescent microscope. The selection generated 12–17 sections per animal and sections on every second slide (7–9 sections per animal) were used for the quantification. After acquisition of digital images of each section, the number of DxRh-labeled axons with an end within 100 μm of the transection line (reaching axons) and the total number of DxRh-labeled axons were manually counted in each section. In a section from a rat 2 h post-surgery, for example, 6 reaching axons per total 160 labeled axons were observed, while 25 reaching axons per total 220 labeled axons were seen in a section from a 4-h-survival rat. The numbers per section were added up in each animal, making 32 reaching axons per 1601 axons labeled in a 2-h-survival rat, for example. Finally, the ratio of the number of reaching axons to the total number of labeled axons was calculated in each animal and was shown as axon number per thousand labeled axons.

2.11. Statistical analyses

For numerical variables, the means and standard errors were calculated. A difference of the mean of number of axons reaching 100 μm of the transection site per thousand labeled axons was compared between two groups (rats surviving 2 h of funiculotomy versus rats surviving 4 h of funiculotomy) using Mann-Whitney *U* test. A p value of <0.05 was considered statistically significant.

3. Results

3.1. Regenerative pioneering axons show a snaking morphology and reach the lesion site within 4 h of a sharp transection with a scalpel

Following transection of the white matter, severed axons immediately retract several hundred micrometers and then promptly start regeneration (Ramon y Cajal, 1928; Kerschensteiner et al., 2005). To know the timing when retracted axons start regeneration, we made a lateral funiculotomy with a scalpel and counted the number of axons whose ends existed within 100 μm of transection site at 2 and 4 h of severance. For a clear identification of severed axonal ends, we differentially labeled them; i.e. caudal ends with dextrans conjugated with tetramethylrhodamine (DxRh) (red) and rostral ones with dextrans conjugated with Alexa Fluor 488 (Dx488) (green) (Fig. 1A-D). To normalize the axon number in terms of labeling efficacy, we further counted a total number of labeled axons and calculated the ratio of number of axons reaching 100 μm of transection site per 1000 labeled axons. The number of DxRh-labeled axons reaching 100 μm (lines, Fig., 1B, 1D) of the transection line was 27.5 ± 2.63 per 1000 labeled axons (mean ± SE, N = 4) in rats 2 h post-surgery and 100.7 ± 3.76 per 1000 labeled axons (N = 3) in rats 4 h post-transection, showing a significant increase in the latter ($p = 0.0285 < 0.05$, Fig. 1F). Thus, axon regeneration had actually occurred within 4 h of funiculotomy in adult rat spinal cord. In addition, some axons had already reached the lesion center within 4 h (arrow, Fig. 1D). Since axons reaching the lesion largely showed a characteristic morphology as snaking or tortuous (arrowheads, Fig. 1E), we calculated the ratio of snaking axons among those reaching 100 μm of the transection site (N = 3, total of 315 axons). The snaking axons occupied 92.0 ± 2.08 percent (Fig. 1G), suggesting that a snaking or tortuous morphology is a typical feature of regenerative pioneering axons.

3.2. The sharp transection forms "axon-glial complex (AGC)" at the lesion site

As we have previously demonstrated (Nishio et al., 2008), a scalpel-transection of adult rat spinal cord frequently produces abnormal axon fragments at the injured white matter, which are highly immunoreactive for high-molecular form neurofilament (NFH-IR). Six hours after a scalpel-transection, many of DxRh-labeled axons reached the lesion site (arrow, Fig. 2A), along which NFH-IR axon fragments clumped together (dotted line, Fig. 2B). The DxRh-labeled axons showing an intermittent snaking (large arrowheads, Fig. 2D) and sprouting from local swellings (arrows and small arrowheads, Fig. 2D) were approaching the aggregates of NFH-IR axon fragments. Thus, we assumed the NFH-IR fragments as a barrier for the regenerative pioneering axons and further examined the fragments in terms of glial involvement or their ultrastructure.

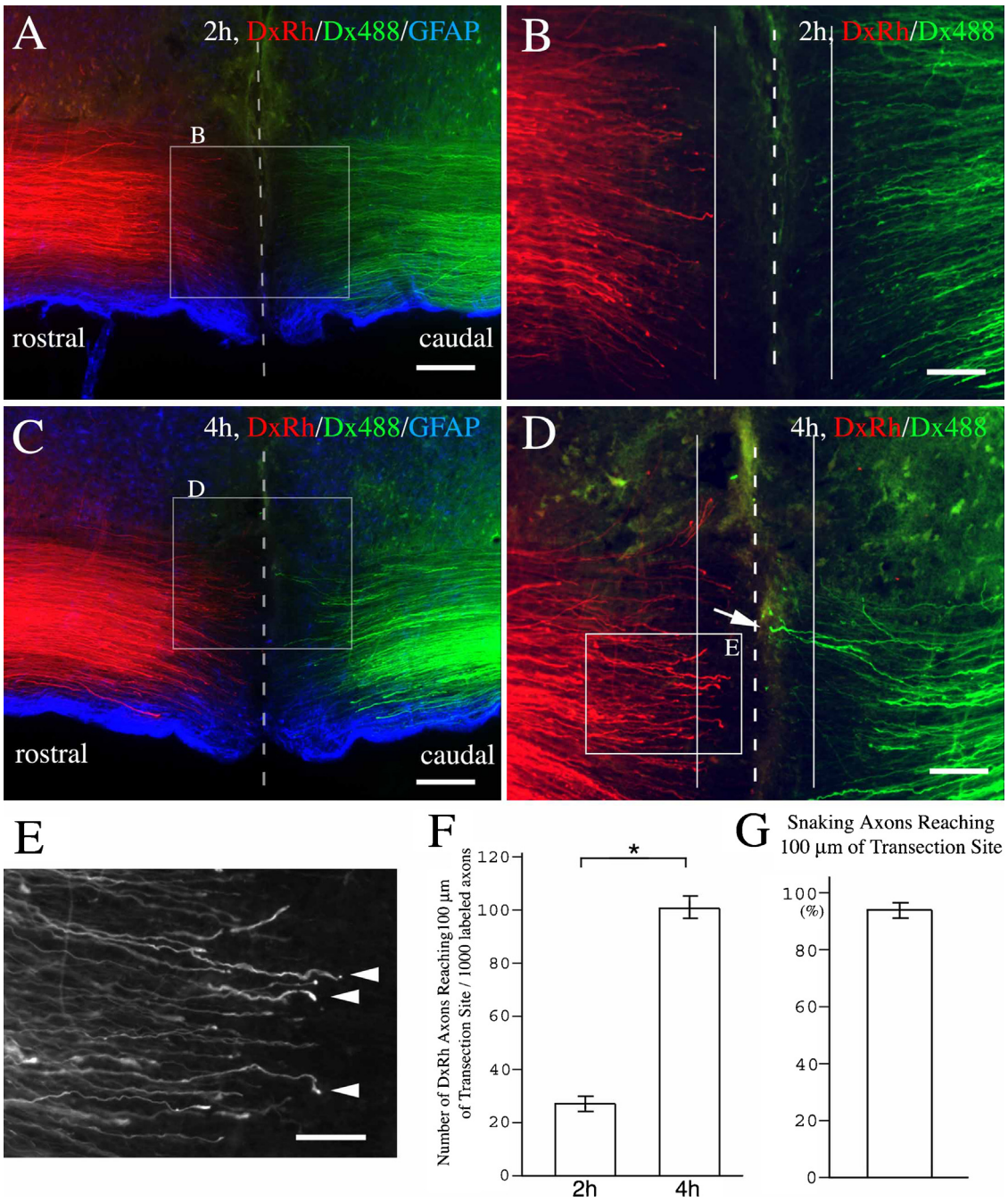

Fig. 1. Regenerative pioneering axons reach the lesion site within 4 h of a sharp transection and show a snaking morphology.
(A–D) Low-power (A, C) and high-power views (B, D) of a representative horizontal section of adult rat spinal cord 2 (A–B) or 4 (C–D) hours after a lateral funiculotomy at T10 level, showing differential labeling [severed axons in the rostral part are labeled with dextrans conjugated with tetramethylrhodamine (DxRh) (red) and axons in the caudal part with dextrans conjugated with Alexa Fluor 488 (Dx488) (green)]. The low-power views (A, C) also show glial fibrillary acidic protein (GFAP)-immunoreactivity (blue). Rostral is to the left hand and caudal to the right hand. Dotted line shows the transection site. Note a clear visualization of both ends indicating the absence of spared axons. Also note that a majority of axonal ends reside over 100 μm away from the transection site. However, some axons had already reached the lesion center 4 h of transection (arrow, D). Scale bars: 250 μm (A, C); 100 μm (B, D). (E) A high-power view of a rectangle in D, showing a characteristic morphology (tortuous or snaking) of "pioneering" axons (arrowheads). Scale bar: 50 μm. (F) The number of DxRh-labeled axons reaching 100 μm of the transection site per thousand labeled axons in rats 2 or 4 h of lateral funiculotomy. The latter shows a significant increase in number (Mann-Whitney *U* test, $p = 0.0285$), indicating a rapid regeneration within 4 h of injury in adult rats. (G) Percentage of "snaking axons" among those reaching 100 μm of the transection site (N = 3, total of 315 axons). Over 90 percent of pioneering axons show a snaking morphology.

Two hours after a scalpel-transection, the NFH-IR axon fragments clumped together along the transection line (arrow, Fig. 3A), which also showed a GFAP-IR expression (arrows, Fig. 3B). Electron microscopy confirmed the aggregation of unmyelinated axons (arrows) at the lesion site (Fig. 3C). High-power views (Fig. 3D–F) revealed that the aggregate was composed of unmyelinated axons and astroglial processes (arrowheads, Fig. 3D). The former were rich in neurofilaments (arrows, Fig. 3F) but had few microtubules (Fig. 3F), as seen in axons receiving a traumatic injury (Pettus et al., 1994; Pettus and Povlishock 1996; Okonkwo et al., 1998), while the latter possessed densely packed intermediate filaments (glial filaments, arrowheads, Fig. 3F) and made a direct contact with the

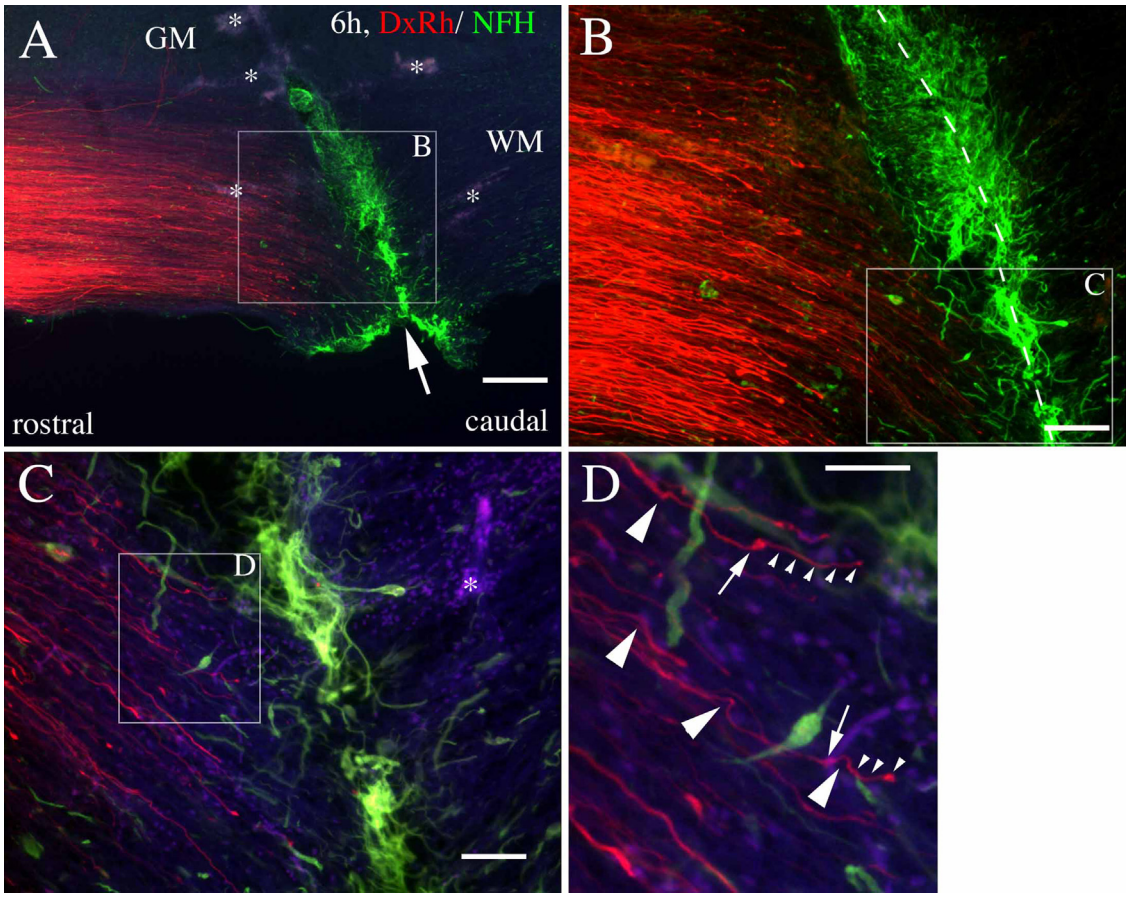

Fig. 2. Regenerative pioneering axons never traverse the aggregate-forming axon segments at the transection site.
(A) A low-power view of a representative horizontal section of adult rat spinal cord 6 h after a lateral funiculotomy, showing axonal labeling (DxRh, red) and NFH-IR (green). Many of DxRh-labeled axons reach the highly NFH-IR axon segments at the transection site (arrow), but never grow across the site. Asterisks show auto-fluorescence from clumps of red blood cells. (B) A high-power view of a rectangle in (A), showing aggregates of NFH-IR axon segments along the transection line (dotted line). (C) A high-power view of a rectangle in (B). (D) A high-power view of a rectangle in (C), showing regenerative pioneering axons near the axon segments. The regenerative pioneering axons are frequently snaking (large arrowheads) and show terminal sprouting (small arrowheads) from a local swelling (arrow). Scale bars; 250 μm (A), 100 μm (B), 50 μm (C), 25 μm (D). Rostral is to the left hand and caudal to the right hand.

axons (Fig. 3F). Therefore, a scalpel-transection of the white matter would immediately produce aggregates of neurofilament-rich axons and astroglial processes, "axon-glial complex (AGC)" at the lesion site, which would be a physicochemical barrier for regenerative pioneering axons.

3.3. *Immediate removal of injured white matter tissue achieves a successful growth of pioneering axons across the tissue-removed lesion*

To verify the hypothesis that the AGC serves as a physicochemical barrier for regenerative pioneering axons, we tested whether an elimination of the AGC would achieve a successful regeneration or not. We tried to surgically eliminate the AGC from the lesion site in lateral funiculotomied rats. More specifically, we made another oblique section immediately after the primary section (lateral funiculotomy), removed the intervening tissue between the 2 sections, surgically eliminated the injured white matter tissue from the lesion edges with a pair of tweezers (debridement), and then gently apposed the open wound, which resulted in making an asymmetric lesion site (Fig. 4A, see Supplementary Video online). Since both sections of the white matter would produce the AGC, the debridement procedure would be essential for the elimination of the AGC. One hour after the surgery, the AGC expressing NFH-IR was locally eliminated from the lesion site (asterisks, Fig. 4B, D), while caudal ends of Dx488-labeled axons were largely observed over 200 μm rostral to the lesion site and never beyond the lesion site (Fig. 4C–D). Four hours after the surgery, the AGC with NFH-IR was locally eliminated from the lesion site (asterisks, Fig. 4E), which was asymmetric with a wider caudal portion (WM, bidirectional arrows, Fig. 4E) due to the secondary oblique section. Importantly, Dx488-labeled axons were seen to grow through the AGC-eliminated area into the distal white matter (380 μm beyond the lesion) making local swellings (arrowheads, Fig. 4H–I) and snaking (arrows, Fig. 4H-I). These axons, regenerative pioneering axons, appeared to grow singly or solitarily along the distal white matter. Thus, the surgical treatments achieved a local elimination of the AGC and successful regeneration across the lesion within 4 h of surgery.

However, the "4 h" appeared extremely short for cut axons to regrow across the lesion site, and we further made a confirmatory experiment; injecting with BSA-coated immobile fluorescent microspheres (Fluoresbrite YG microsphere, 3 μm in size) into the debrided lesion (Fig. 5A–c) to mark the lesion site. Four hours after the surgical treatments, the lesion site was clearly identified by a line of fluorescent microspheres (arrow, Fig. 5B), from which DxRh-labeled axons (arrows, Fig. 5C) grew into the distal white matter (350 μm beyond the lesion) showing an intermittent snaking (arrowheads, Fig. 5C). Therefore, it was concluded that the AGC-eliminating surgery could allow regenerative pioneering axons to grow across the lesion only within 4 h of the surgery.

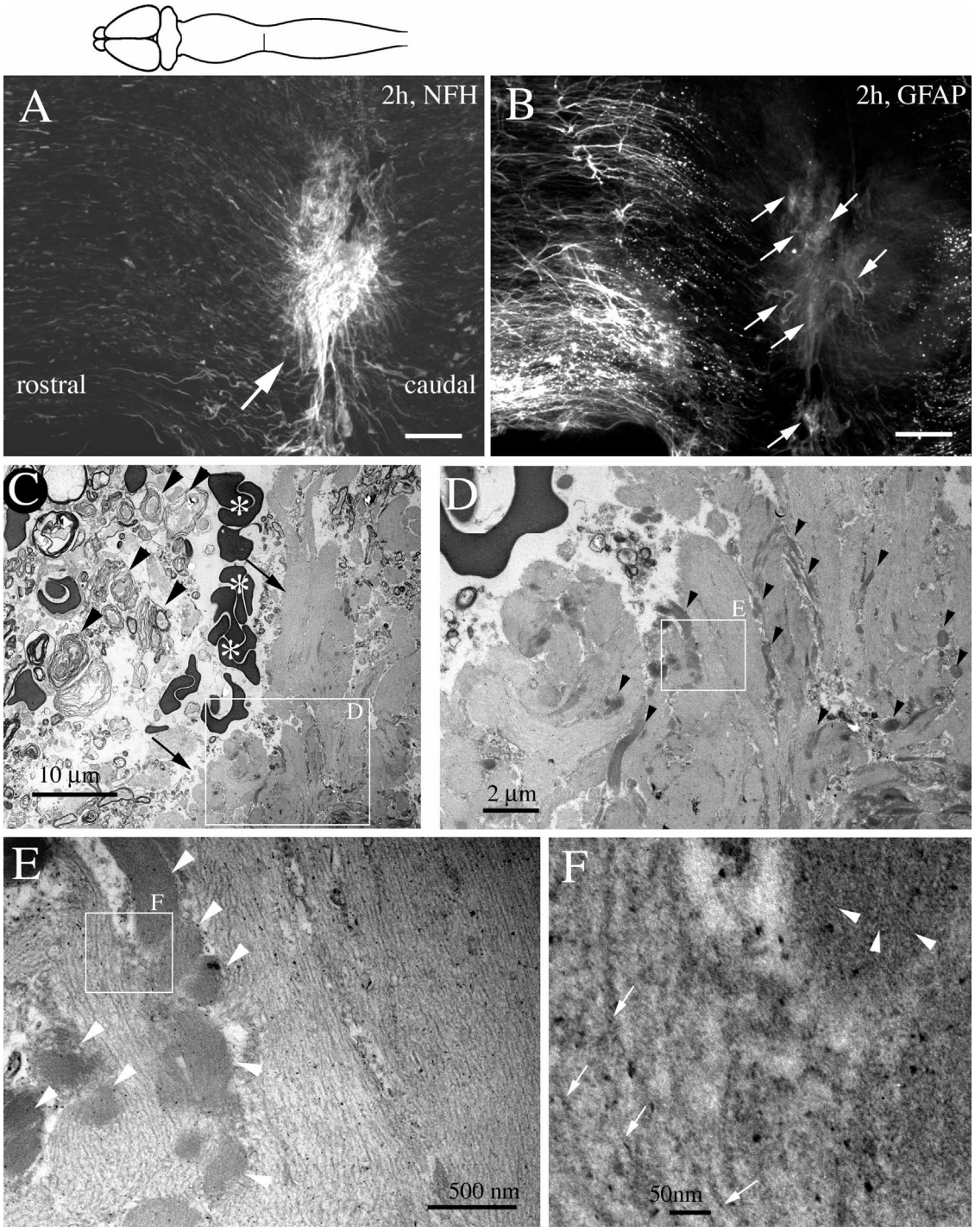

Fig. 3. Transection of the white matter immediately generates aggregates of axon-glial complex (AGC).
(A–B) A low-power view of a representative horizontal section of adult rat spinal cord 2 h after a lateral funiculotomy, showing high molecular form neurofilament-like immunoreactivity (NFH-IR) (A) and glial fibrillary acidic protein-like immunoreactivity (GFAP-IR) (B). The highly NFH-IR axon segments (arrow, A) form an aggregate at the transection site, which also express GFAP-IR (arrows, B). (C) An electron microscopic view of the lesion site 2 h after funiculotomy. Note clusters of myelin debris (arrowheads), red blood cells (asterisks), and unmyelinated axons (arrows) at the lesion site. (D) A high-power view of a rectangle in (C). Unmyelinated axons form an aggregate, in which electron-denser processes (arrowheads) are involved. (E) A high-power view of a rectangle in (D). The electron denser processes (arrowheads) make a direct contact with unmyelinated axons. (F) A high-power view of a rectangle in (E). The electron denser processes contain densely packed intermediate filaments (glial filament, arrowheads), while the unmyelinated axons have many intermediate filaments (neurofilaments, arrows) and few microtubules. Scale bars; 250 μm (A, B), 10 μm (C), 2 μm (D), 500 nm (E), 50 nm (F).

3.4. Regenerative axons form a fascicle within 24 h of funiculotomy

In axonogenesis during development of the CNS, follower axons are known to fasciculate or form a fascicle with pioneer axons (Bak and Fraser, 2003). Since the AGC-eliminating surgery could allow regenerative pioneering axons to grow across the lesion, we next examined whether later coming followers would also make a fascicle in regeneration or not. We examined the lesion site 24 h after the AGC-eliminating surgery. At the time of surgery, we

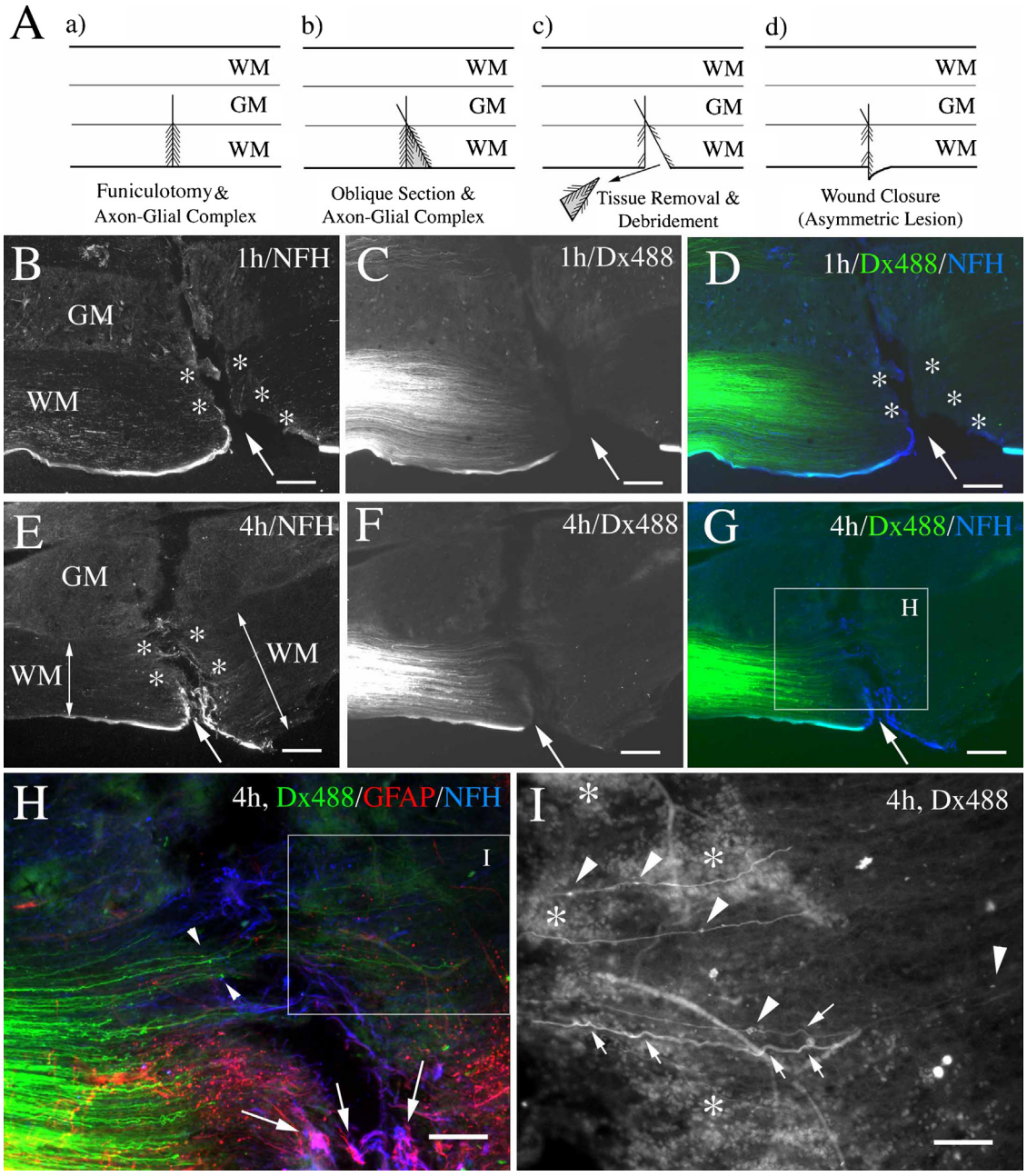

Fig. 4. Immediate removal of injured white matter tissue achieves a successful growth of pioneering axons across the tissue-removed lesion.
(A) Schematic representation of surgical procedures. A left lateral funiculotomy with a scalpel produces an axon-glial complex (AGC, shaded area, a) at the lesion site. Additional oblique section (b), a removal of the intervening tissue and debridement of the stump surface (c) are followed by a closure of the open wound to make an asymmetric lesion site (d). (B–D) A low-power view of a representative horizontal section of adult rat spinal cord 1 h after the surgery, showing NFH-IR (B, D) and Dx488 labeling (C–D). Note an elimination of NFH-IR-positive AGC (asterisks) from the lesion site (arrow). Also note that Dx488-labeled axons do not extend across the lesion site. (E–G) A low-power view of a representative horizontal section of adult rat spinal cord 4 h after the surgery, showing NFH-IR (E, G) and Dx488 labeling (F–G). Note a local elimination of NFH-IR-positive AGC (asterisks) from the lesion site (arrow), which is asymmetric with a wider tract in the caudal (WM). (H) A high-power view of a rectangle in G, showing triple labeling with Dx488, GFAP-IR, and NFH-IR. Note that Dx488-labeled axons containing local swellings (arrowheads) grow across the lesion site through the AGC-eliminated area. Arrows indicate a remnant of the AGC that was spared from surgical debridement. (I) A high-power view of a boxed area in H, showing Dx488-labeling. Those axons solitarily grow showing intermittent snaking (arrows) and local swellings (arrowheads). Asterisks indicate auto-fluorescence from red blood cells. Scale bars; 250 μm (B-G), 100 μm (H), 50 μm (I). Abbreviations: GM, gray matter; WM, white matter.

further inserted an epoxy-based sheet with pores (Fig. 6B, 19.6 μm-thick, pore size was 125 μm in diameter) into the tissue-removed lesion (Fig. 6A) to mark the lesion site. Twenty-four hours after the surgery, Dx488-labeled axons had successfully regenerated across the sheet (S, Fig. 6D) 2 mm beyond the lesion site (Fig. 6C). The regenerative axons had grown through an AGC-eliminated (GFAP-IR-free) area (asterisks, Fig. 6D), while they appeared to stop growing (large arrowheads, Fig. 6D) near the GFAP-IR AGC (large arrows, Fig. 6D) that was spared from the surgical debridement. In addition, GFAP-IR astroglial processes (small arrows, Fig. 6D) frequently surrounded the epoxy-based sheet (S, blue-colored or dot-lined, Fig. 6D), which was split into fragments at the time of tissue slicing with a microtome. Interestingly, a few dozen axons converged on a pore site of the sheet (asterisks, Fig. 6D), but then diverged after leaving the pore and re-entering the white matter (Fig. 6E). Among axons that grew along the distal white mat-

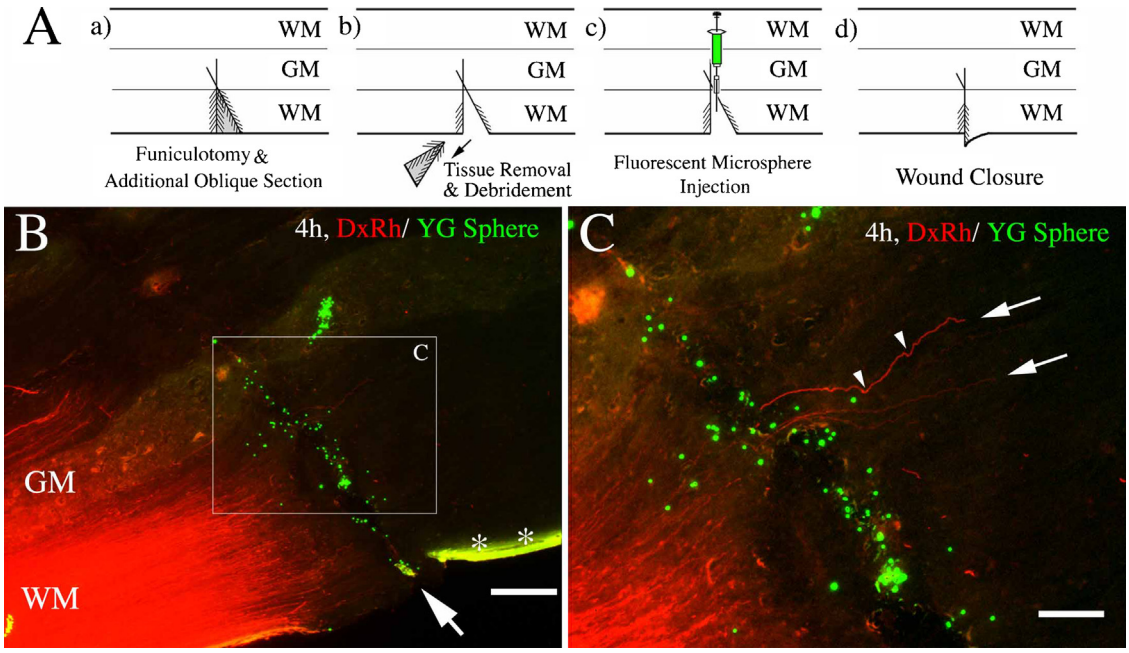

Fig. 5. An AGC-eliminating surgery achieves a successful growth of pioneering axons across the tissue-removed & microsphere-injected lesion.
(A) Schematic representation of surgical procedures. A left lateral funiculotomy and additional oblique section produce a triangular pyramid with AGC (a). A removal of the intervening tissue and debridement of the stump surface (b) are followed by a local injection of BSA-coated fluorescent microspheres into the tissue-removed space to mark the transection (c), and a wound closure (d). (B) A low-power view of a representative horizontal section of adult rat spinal cord 4 h after the surgery, showing axonal labeling with DxRh and YG spheres. Note the transection site (arrow, B) that is marked with a line of YG microspheres. Asterisks show auto-fluorescence from a surgical adhesive. (C) A high-power view of a rectangle in B. Note DxRh-labeled axons (arrows) growing from the line of YG spheres. They are also intermittently snaking (arrowheads). Scale bars; 250 μm (B), 100 μm (C). Abbreviations: GM, gray matter; WM, white matter; BSA, bovine serum albumin.

ter (Fig. 6E), some appeared to grow solitarily (arrows) but the others appeared to follow the trajectory of a predecessor (arrowheads). Thus, the former were considered pioneers and the latter were followers, and it appeared likely that the regenerative axons had already formed several fascicles 24 h after a funiculotomy. In addition, the former showed a characteristic snaking morphology (Fig. 6E).

To confirm axonal fascicle formation in an early stage of regeneration, we further examined the ultrastructure of axons growing across a pore of the sheet 24 h post-surgery by using electron microscopy (Fig. 6F–G). A bundle of unmyelinated axons were seen to grow around the sheet (arrowheads, Fig. 6F). A high-power view revealed that the shafts of unmyelinated axons (Ax, Fig. 6G) and a growth cone containing an electron-dense material (arrowhead, Fig. 6G) directly contacted with each other forming a fascicle, suggesting a contact-based guidance mechanism in regeneration of followers. In addition, thin astroglial processes (arrows, Fig. 6G) also made a direct contact with the shaft of unmyelinated axons. Thus, it was demonstrated that fasciculation of regenerative axons actually took place in adult spinal cords 24 h after injury.

4. Discussion

In the present study, we generated a hypothesis that the abnormal axon segments (or axon-glial complex; AGC) at the lesion site is a barrier for the regenerative pioneering axons, and verified the hypothesis by developing a novel surgical procedure to eliminate the AGC. Fortunately, we achieved a partial elimination of the AGC from the lesion site, across which regenerative axons rapidly and successfully extended into the distal white matter in adult rats.

4.1. Bona fide regeneration of axons; exclusion of axon sparing

Axon sparing comes often to an issue in studies showing axon regeneration after spinal cord injury (Steward et al., 2003) and the present results of successful axon growth within hours of the transection was faster than expected. Thus, we made several confirmatory treatments to exclude axonal sparing. First, we sectioned the cord twice (duplicated sections) and removed the injured white matter tissue under a visual guidance, which allowed us to confirm a definite separation of the lateral funiculus. Second, the additional section we made was oblique to the longitudinal axis of the cord and the resulting lesion site became asymmetric across the lesion with a broader tract in the caudal. If axons grow through the asymmetric lesion site, they cannot be spared. Third, an injection of BSA-coated immobile fluorescent microspheres into the tissue-removed lesion allowed us to confirm the history of tissue separation. Fourth, an insertion of an epoxy-based sheet into the tissue-removed lesion also allowed us to confirm the history of tissue separation. If axons grow through the artificial material, they cannot be spared (Steward et al., 2003). In addition, axons that had traversed the lesion showed a characteristic snaking morphology or making multistep sprouts with local swellings. We further confirmed ultrastructure of regenerative axons in electron microscopy. Taken together, those axons penetrating the lesion could not be intact, but be regenerative.

4.2. Rapid axonal responses after axotomy

After an axotomy in cultured neurons, it takes 30–60 s to reseal the severed axonal ends (Sahly et al., 2006) and takes 30 min to transform into a growth cone (Verma et al., 2005; Sahly et al., 2006). After a transection of the cord in adult mice, an *in vivo* imaging has shown that severed axons die back 200–300 μm from the lesion site

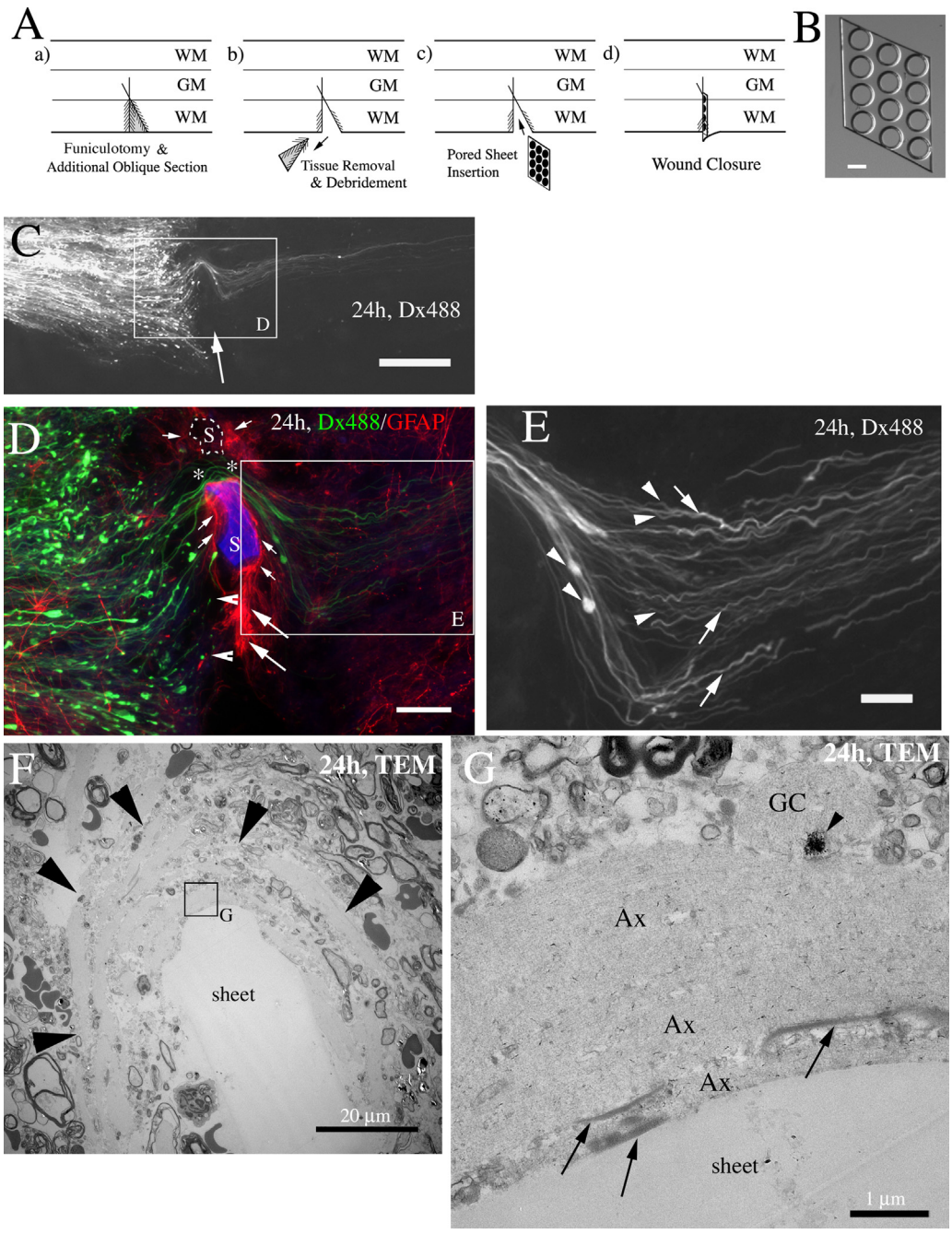

Fig. 6. Regenerative axons form a fascicle within 24 h of funiculotomy.
(A) Schematic representation of surgical procedures. Duplicated cord sections produce a triangular pyramid with the AGC (a). A removal of the intervening tissue and debridement of the stump surface (b) are followed by a local insertion of a pored sheet (c) and a wound closure (d). Abbreviations: GM, gray matter; WM, white matter. (B) A phase-contrast image of an epoxy-based sheet. (C) A low-power view of a horizontal section of adult rat spinal cord 24 h after the surgery, showing axonal labeling with Dx488. Dx488-labeled axons grow 2 mm beyond the lesion site (arrow) forming fascicles. (D) A high-power view of rectangle in (C), showing Dx488 labeling (green) and GFAP-IR (red). Fragments of the sheet are labeled as 'S' (blue-colored or dot-lined). Note a remnant of the AGC with GFAP-IR (large arrows) that was spared from the surgical debridement and a successful elimination of the AGC (asterisks). Dx488-labeled axons stagnate at the AGC (large arrowheads), while they extend across the lesion through the AGC-eliminated area (asterisks). Also note GFAP-IR astroglial processes (small arrows) surrounding the sheet as a foreign body reaction. (E) A high-power view of rectangle in (D), showing Dx488 labeling. Note a fascicle formation by followers (arrowheads) following a trajectory of the predecessor (pioneers, large arrows). (F) An electron microscopic image of the sheet-inserted lesion site 24 h after the surgery. Note fascicles of unmyelinated axons (arrowheads) extending around the sheet. (G) A high power-image of rectangle in (F) shows a direct contact of unmyelinated axons (Ax) with themselves, astroglial processes (arrows), and the sheet surface. Note that a growth cone (GC) containing an electron dense material (arrowhead) also makes a direct contact with a shaft of unmyelinated axon, suggesting contact-based axon guidance in followers. Scale bars; 500 μm (C), 100 μm (D), 50 μm (E), 20 μm (F), 1 μm (G).

within 30 min of surgery (Kerschensteiner et al., 2005). In addition, severed axons grow normally for 2–5 hours in the presence of protein synthesis inhibitor in culture (Shaw and Bray, 1977; Campbell and Holt, 2001; Leung et al., 2006), suggesting autonomy of initial axonal growth. As a calculation taking these into account, severed axons would start regrowth as early as 1 h after a cord section at 200 μm from the lesion site. If such quickly regenerating axons reached the lesion site 4 h of transection, the provisional growth rate along the proximal white matter tracts would be calculated as 200 μm per 3 h (about 66 μm/hour). Therefore, the present results

suggest that the regenerative pioneering axons grow along the proximal white matter tracts at a maximum rate of 66 μm/hour. The calculated rate of axonal growth may seem extremely rapid. However, the high rate of axonal growth along mature white matter can well be explained by axonal navigation mechanisms (Tessier-Lavigne and Goodman 1996; Dickson 2002) and it is possible that the regenerative axons, if a barrier is omitted, could advance in such a rapid speed along the repellent-surrounded roads like a Maglev car, since mature CNS white matter has ready-made tracks that are surrounded by strong repellents, myelin-associated proteins (Raisman, 2004). In support of this idea, the rapid growth of axons at the rate of over 1 mm/day along the white matter tracts of adult rat spinal cord has been reported in neurons that were transplanted into the white matter (Davies et al. in 1999).

4.3. Axon-glial complex (AGC) as a barrier for regenerative axons

We previously reported an emergence of highly NF-IR axon segments at the scalpel-transection site of the cord in adult rats (Nishio et al., 2008). Severed axonal ends at the transection site showed a rapid enhancement in NFH-IR expression within 5 min of injury, which conversely lost beta-III tubulin-IR. These events were followed by a secondary axotomy near the transection site, which finally formed abnormal zipper-like axon segments (fragments) at the transection site. Povlishock and co-workers have reported a similar axonal pathology immediately after a traumatic brain injury as a focal axonal injury, which includes a focal perturbation of axolemmal permeability, a rapid compaction of axonal neurofilament, an enhanced expression of NF-IR and a microtubular loss (Pettus et al., 1994; Pettus and Povlishock 1996; Okonkwo et al., 1998). The present study further confirmed the abundance of neurofilaments and poverty of microtubules in the abnormal axon segments by an electron microscopy. In addition, this study revealed that the abnormal axon segments were made up of aggregates of unmyelinated axons and astroglial processes (axon-glial complex, AGC). In the white matter, astrocytes give off numerous longitudinal processes that insert themselves between and along the length of axons (Suzuki and Raisman, 1992). Upon transection of the white matter with a scalpel, a mechanical compression by a scalpel on both axons and glial processes would anchor the glial processes to axons, and hence generate an aggregate of AGC. In the AGC-eliminating surgery, we added another section of the white matter, which would also generate the AGC along a trajectory of the second section. Thus, a removal of the injured white matter tissue or debridement (cleaning) of the lesion site was considered an essential step to eliminate the AGC. Under these treatments, the NFH-IR AGC was locally eliminated from the lesion site and axons successfully regenerated through the AGC-eliminated area, suggesting that the surgical procedure could effectively eliminate the AGC and that the AGC was a barrier for axon regeneration.

In conclusion, the present study for the first time demonstrated a rapid and direct axonal growth across the lesion site in adult rat spinal cord receiving a focal removal of the white matter tissue. The limited axon regeneration in mature mammalian CNS has been partly attributed to a reduced capacity of mature CNS neurons to regenerate axons (Sun and He, 2010; Yang and Yang, 2012). Contrary to this notion, the present results indicate that mature CNS axons, under adequate conditions, can rapidly regenerate across the lesion site without control of a neuronal cell body at least during an initial active phase of regeneration. In addition, the present study may lead to a novel treatment in a future to induce successful axon regeneration by removing a scar tissue and rejoining the severed cord in chronically spinal cord injured patients.

Author contributions

All authors participated in designing experiments. T.N. carried out experiments. T.N. & H.F. analyzed the data, and wrote the main manuscript text. I. K. participated in making the epoxy-based sheets with pores. All authors contributed to the final version of the manuscript.

Additional information

Competing financial interests: The authors declare no competing financial interests.

Acknowledgements

This work was supported by Japan Society for the Promotion of Science (JSPS) (Grant-in Aid for Challenging Exploratory Research 25670644, 15K15550) and Funding for Collaborative Research with Institute for Frontier Medical Sciences, Kyoto University. The author (T. N.) would like to express the deepest appreciation to Miss Rieko Takai for useful comments and encouragement throughout this study.

Appendix A. Supplementary data

Supplementary data associated with this article can be found, in the online version, at https://doi.org/10.1016/j.neures.2017.10.011.

References

Bak, M., Fraser, S.E., 2003. Axon fasciculation and differences in midline kinetics between pioneer and follower axons within commissural fascicles. Development 130, 4999–5008.
Busch, S.A., Silver, J., 2007. The role of extracellular matrix in CNS regeneration. Curr. Opin. Neurobiol. 17, 120–127.
Campbell, D.S., Holt, C.E., 2001. Chemotropic responses of retinal growth cones mediated by rapid local protein synthesis and degradation. Neuron 32, 1013–1026.
Davies, S.J., Goucher, D.R., Doller, C., Silver, J., 1999. Robust regeneration of adult sensory axons in degenerating white matter of the adult rat spinal cord. J. Neurosci. 19, 5810–5822.
Dickson, B.J., 2002. Molecular mechanisms of axon guidance. Science 298, 1959–1964.
Iseda, T., Nishio, T., Kawaguchi, S., Kawasaki, T., Wakisaka, S., 2003. Spontaneous regeneration of the corticospinal tract after transection in young rats: collagen type IV deposition and astrocytic scar in the lesion site are not the cause but the effect of failure of regeneration. J. Comp. Neurol. 464, 343–355.
Iseda, T., Nishio, T., Kawaguchi, S., Yamamoto, M., Kawasaki, T., Wakisaka, S., 2004. Spontaneous regeneration of the corticospinal tract after transection in young rats: a key role of reactive astrocytes in making favorable and unfavorable conditions for regeneration. Neuroscience 126, 365–374.
Kawasaki, T., Nishio, T., Kurosawa, H., Roder, J., Jeromin, A., 2003. Spatiotemporal distribution of neuronal calcium sensor-1 in the developing rat spinal cord. J. Comp. Neurol. 460, 465–475.
Kerschensteiner, M., Schwab, M.E., Lichtman, J.W., Misgeld, T., 2005. In vivo imaging of axonal degeneration and regeneration in the injured spinal cord. Nat. Med. 11, 572–577.
Leung, K.M., van Horck, F.P., Lin, A.C., Allison, R., Standart, N., Holt, C.E., 2006. Asymmetrical beta-actin mRNA translation in growth cones mediates attractive turning to netrin-1. Nat. Neurosci. 9, 1247–1256.
Nishio, T., Kawaguchi, S., Yamamoto, M., Iseda, T., Kawasaki, T., Hase, T., 2005. Tenascin-C regulates proliferation and migration of cultured astrocytes in a scratch wound assay. Neuroscience 132, 87–102.
Nishio, T., Kawaguchi, S., Fujiwara, H., 2008. Emergence of highly neurofilament-immunoreactive zipper-like axon segments at the transection site in scalpel-cordotomized adult rats. Neuroscience 155, 90–103.
Okonkwo, D.O., Pettus, E.H., Moroi, J., Povlishock, J.T., 1998. Alteration of the neurofilament sidearm and its relation to neurofilament compaction occurring with traumatic axonal injury. Brain Res. 784, 1–6.
Pettus, E.H., Povlishock, J.T., 1996. Characterization of a distinct set of intra-axonal ultrastructural changes associated with traumatically induced alteration in axolemmal permeability. Brain Res. 722, 1–11.
Pettus, E.H., Christman, C.W., Giebel, M.L., Povlishock, J.T., 1994. Traumatically induced altered membrane permeability: its relationship to traumatically induced reactive axonal change. J. Neurotrauma 11, 507–522.

Raisman, G., 2004. Myelin inhibitors: does no mean go? Nat. Rev. Neurosci. 5, 157–161.
Ramon y Cajal, S., 1928. Degeneration and Regeneration in the Nervous System. New York, Hafner.
Sahly, I., Khoutorsky, A., Erez, H., Prager-Khoutorsky, M., Spira, M.E., 2006. On-line confocal imaging of the events leading to structural dedifferentiation of an axonal segment into a growth cone after axotomy. J. Comp. Neurol. 494, 705–720.
Schwab, M.E., Strittmatter, S.M., 2014. Nogo limits neural plasticity and recovery from injury. Curr. Opin. Neurobiol. 27, 53–60.
Sharma, K., Selzer, M.E., Li, S., 2012. Scar-mediated inhibition and CSPG receptors in the CNS. Exp. Neurol. 237, 370–378.
Shaw, G., Bray, D., 1977. Movement and extension of isolated growth cones. Exp. Cell Res. 104, 55–62.
Silver, J., Miller, J.H., 2004. Regeneration beyond the glial scar. Nat. Rev. Neurosci. 5, 146–156.
Sun, F., He, Z., 2010. Neuronal intrinsic barriers for axon regeneration in the adult CNS. Curr. Opin. Neurobiol. 20, 510–518.
Steward, O., Zheng, B., Tessier-Lavigne, M., 2003. False resurrections: distinguishing regenerated from spared axons in the injured central nervous system. J. Comp. Neurol. 459, 1–8.
Suzuki, M., Raisman, G., 1992. The glial framework of central white matter tracts: segmented rows of contiguous interfascicular oligodendrocytes and solitary astrocytes give rise to a continuous meshwork of transverse and longitudinal processes in the adult rat fimbria. Glia 6, 222–235.
Tessier-Lavigne, M., Goodman, C.S., 1996. The molecular biology of axon guidance. Science 274, 1123–1133.
Verma, P., Chierzi, S., Codd, A.M., Campbell, D.S., Meyer, R.L., Holt, C.E., Fawcett, J.W., 2005. Axonal protein synthesis and degradation are necessary for efficient growth cone regeneration. J. Neurosci. 25, 331–342.
Yang, P., Yang, Z., 2012. Enhancing intrinsic growth capacity promotes adult CNS regeneration. J. Neurol. Sci. 312, 1–6.